Monthly Notices
of the
ROYAL ASTRONOMICAL SOCIETY

MNRAS **429,** 1695–1704 (2013) doi:10.1093/mnras/sts455

On the rapid demise of Ly α emitters at redshift $z \gtrsim 7$ due to the increasing incidence of optically thick absorption systems

James S. Bolton[1,2]⋆ and Martin G. Haehnelt[3]

[1]*School of Physics and Astronomy, University of Nottingham, University Park, Nottingham NG7 2RD*
[2]*School of Physics, University of Melbourne, Parkville, VIC 3010, Australia*
[3]*Kavli Institute for Cosmology and Institute of Astronomy, Madingley Road, Cambridge CB3 0HA*

Accepted 2012 November 20. Received 2012 November 19; in original form 2012 August 21

ABSTRACT

A variety of independent observational studies have now reported a significant decline in the fraction of Lyman-break galaxies which exhibit Lyα emission over the redshift interval $z = 6$–7. In combination with the strong damping wing extending redward of Lyα in the spectrum of the bright $z = 7.085$ quasar ULAS 1120+0641, this has strengthened suggestions that the hydrogen in the intergalactic medium (IGM) is still substantially neutral at $z \sim 7$. Current theoretical models imply H I fractions as large as 40–90 per cent may be required to explain these data assuming there is no intrinsic evolution in the Lyα emitter population. We propose that such large neutral fractions are not necessary. Based on a hydrodynamical simulation which reproduces the absorption spectra of high-redshift ($z \sim 6$–7) quasars, we demonstrate that the opacity of the intervening IGM redward of rest-frame Lyα can rise rapidly in average regions of the Universe simply because of the increasing incidence of absorption systems which are optically thick to Lyman continuum photons as the tail-end of reionization is approached. Our simulations suggest that these data do not require a large change in the IGM neutral fraction by several tens of per cent from $z = 6$ to 7, but may instead be indicative of the rapid decrease in the typical mean free path for ionizing photons expected during the final stages of reionization.

Key words: galaxies: high-redshift – intergalactic medium – quasars: absorption lines – dark ages, reionization, first stars.

1 INTRODUCTION

The opacity observed blueward of rest-frame Lyα in the spectra of distant quasars rises towards higher redshifts (Fan et al. 2006; Becker, Rauch & Sargent 2007), indicating that the fraction of neutral hydrogen in the intergalactic medium (IGM) is small but increasing with look-back time. This observation, coupled with the Thomson optical depth measured from cosmic microwave background data (Komatsu et al. 2011), suggests that an extended epoch of hydrogen reionization was ending by $z \sim 6$–7. Reaching further into the epoch of reionization – when intergalactic hydrogen is still substantially neutral – is difficult, but Lyα selected galaxies may offer one promising route to probing somewhat deeper into this distant era (Miralda-Escudé & Rees 1998; Haiman 2002). The increasing H I content in the IGM at $z > 6$ produces a Lyα damping wing which can extend redward of a galaxy's Lyα emission line. The damping wing reduces the visibility of the Lyα emission (Miralda-Escudé 1998), and the number of Lyα emitting galaxies (LAEs) observed in flux-limited surveys will thus decrease as the ambient H I fraction rises with increasing redshift (Haiman & Spaans 1999).

The resonant nature of the Lyα transmission unfortunately complicates this simple picture. Source clustering (Furlanetto, Zaldarriaga & Hernquist 2006), dust (Hansen & Oh 2006; Dayal, Maselli & Ferrara 2011) and resonant Lyα scattering within the sources themselves – which is sensitive to both the H I content and gas velocities (Santos 2004; Dijkstra & Wyithe 2010) – all impact on the visibility of Lyα emission. The complex resonant radiative transfer within the galaxies often leads to substantial line redshifts of several hundred km s^{-1} which can significantly enhance the visibility of LAEs when the surrounding IGM is still substantially neutral (Barnes et al. 2011; Dijkstra, Mesinger & Wyithe 2011; Laursen, Sommer-Larsen & Razoumov 2011; Zheng et al. 2011; Jeeson-Daniel et al. 2012).

Recently, however, a significant decrease in the transmission of Lyα photons from high-redshift galaxies has been found between $z = 6$ and 7 (Stark et al. 2010; Hayes et al. 2011; Pentericci et al. 2011; Curtis-Lake et al. 2012; Ono et al. 2012; Schenker et al. 2012). This result is based on the rapid decline in the fraction of Lyman-break galaxies (LBGs) which exhibit Lyα emission – a quantity

⋆ E-mail: james.bolton@nottingham.ac.uk

which is (in principle) less susceptible than the LAE luminosity function (e.g. Malhotra & Rhoads 2004; Kashikawa et al. 2006; Hu et al. 2010) to observational selection effects and intrinsic evolution in the LAE population. Based on comparisons to existing numerical simulations and semi-numerical models of reionization, the reported rapid decrease in the transmission of Lyα emission at $z \sim 6$–7 may be interpreted as a rapid change in the volume-averaged neutral fraction (by several tens of per cent) over a rather short redshift interval (Pentericci et al. 2011; Ono et al. 2012; Schenker et al. 2012).

Such a rapid change in the neutral fraction is, however, at odds with the rather low ionizing emissivity suggested by the Lyα forest data at $z = 5$–6 (Bolton & Haehnelt 2007b) which appears to imply a much slower evolution of the neutral fraction. Theoretical reionization models matching the Lyα forest data (e.g. Ciardi et al. 2012; Jensen et al. 2012; Kuhlen & Faucher-Giguère 2012) therefore have considerable difficulty in explaining the rather large neutral fractions (∼40–90 per cent) that have been inferred from the recent LAE/LBG observations at $z \sim 7$. Alternative explanations which – either individually or in combination – might allow for a more modest change in the IGM neutral fraction include an increase in the escape fraction of ionizing photons, or an increase in the interstellar dust content of the galaxies towards higher redshift (see Forero-Romero et al. 2012 for further discussion of these points).

In this paper, we shall argue that one other clue to this puzzle is provided by the quasar ULAS J1120+0641 at $z = 7.085$, recently discovered by the United Kingdom Infrared Telescope (UKIRT) Infrared Deep Sky Survey (UKIDSS; Lawrence et al. 2007). The spectrum of ULAS J1120+0641 exhibits a strong Lyα damping wing extending redward of the quasar Lyα emission line (Mortlock et al. 2011) – exactly what is needed to suppress the generally redshifted (relative to the systemic redshift of the galaxy) emission of LAEs. Theoretical models predict that the regions surrounding rare, bright quasars are amongst the first to reionize (e.g. Furlanetto, Zaldarriaga & Hernquist 2004; Iliev et al. 2006; McQuinn et al. 2007b; Trac & Cen 2007; Zahn et al. 2007). If the environment around ULAS J1120+0641 is typical of quasar host galaxies at $z > 7$, the significantly weaker ionizing radiation field expected around even the brightest LAEs implies that the impact of the red Lyα damping wing on LAE visibility should be even stronger.

Bolton et al. (2011) used high-resolution simulations of Lyα absorption to demonstrate that unless a proximate damped Lyα absorber lies within ∼5 pMpc of the quasar, a volume-averaged H I fraction of at least $\langle f_{\rm H\,I}\rangle_{\rm V} = 0.1$ is required to reproduce the damping wing observed around ULAS J1120+0641. In this work, we show that an H I fraction of around 10 per cent could also explain the rapid evolution of the LAEs – obviating the need for H I fractions as large as 40–90 per cent. The difference in the inferred neutral fraction is due to the inclusion of small-scale (∼20 pkpc), optically thick absorption systems which remain unresolved in large-scale ($\gtrsim$100 cMpc) reionization simulations. On including these systems, the Lyα opacity up to a few hundred km s^{-1} redward of rest-frame Lyα rises more rapidly with H I fraction than usually predicted. As we shall demonstrate, this is because the intervening Lyα opacity of the IGM at the end of hydrogen reionization is strongly affected by the increasing size of these systems, which naturally occurs as the metagalactic photoionization rate decreases. A more modest neutral fraction of ∼10 per cent is much easier to reconcile with the fact that quasar absorption spectra at $z \simeq 6$ appear to indicate that the IGM is highly ionized only 180 Myr later (Fan et al. 2006; Wyithe, Bolton & Haehnelt 2008, but see also Mesinger 2010).

We begin our analysis in Section 2, where we describe our modelling of the IGM Lyα opacity and the procedure we adopt for incorporating self-shielded gas into a hydrodynamical simulation. In Section 3, the properties of the optically thick absorbers in the simulations are discussed in more detail. We explore the implications of these absorption systems for the visibility of Lyα emission from galaxies in Section 4, and we conclude in Section 5. We assume the cosmological parameters $\Omega_{\rm m} = 0.26$, $\Omega_\Lambda = 0.74$, $\Omega_{\rm b}\,h^2 = 0.023$, $h = 0.72$ and a helium mass fraction of $Y = 0.24$ throughout. Comoving and proper distances are denoted by using the prefixes 'c' and 'p', respectively.

2 NUMERICAL SIMULATIONS OF THE IGM

2.1 Hydrodynamical model

We model the IGM using a high-resolution hydrodynamical simulation performed with the parallel TreeSPH code GADGET-3, last described in Springel (2005). The simulation employs a box size of $10\,h^{-1}$ cMpc, a gas particle mass of $9.2 \times 10^4\,h^{-1}\,{\rm M}_\odot$ and a gravitational softening length of $0.65\,h^{-1}$ ckpc. The gas is reionized instantaneously by a uniform, optically thin ionizing background at $z = 9$ based on the Haardt & Madau (2001) galaxies and quasars emission model. Although we subsequently recompute the ionization state of the gas, this means that the IGM density field at $z \leq 9$ is already Jeans smoothed by the increased gas pressure following photoheating (e.g. Pawlik, Schaye & van Scherpenzeel 2009). This simulation was previously used to model the Lyα opacity in the near zone of the high-redshift quasar ULAS J1120+0641 at $z = 7.085$ (Bolton et al. 2011). In this work, we use an output at $z = 7$.

The initial equilibrium ionization state of the gas is set by a spatially uniform ionizing background. We do not model the patchy ionization state of the IGM by following the radiative transfer of ionizing photons emitted by individual sources. We will, however, estimate the effect of a central source on the ionization state of the IGM later in our analysis. A box size of $10\,h^{-1}$ cMpc is in any case too small to correctly capture the large-scale topology of the reionization process. Instead, the high-mass resolution of the simulation allows us to incorporate the small-scale structures responsible for optically thick absorption systems. These absorption systems are expected to define the edge of ionized bubbles (Crociani et al. 2011), regulate the mean free path at overlap (Miralda-Escudé, Haehnelt & Rees 2000; Gnedin & Fan 2006; McQuinn, Oh & Faucher-Giguère 2011) and delay the latter stages of reionization (Ciardi et al. 2006; Alvarez & Abel 2012). These systems remain unresolved in most large-scale reionization simulations (but see Choudhury, Haehnelt & Regan 2009; Crociani et al. 2011; Alvarez & Abel 2012 for recent 'semi-numerical' approaches, and Gnedin & Fan 2006; Kohler & Gnedin 2007; Altay et al. 2011; McQuinn et al. 2011 for smaller simulations which resolve self-shielded systems) and are therefore often not considered when estimating the impact of intergalactic Lyα absorption on the visibility of LAEs.

2.2 Modelling optically thick absorption systems

In order to include optically thick absorbers in our model, following Schaye (2001) we use a simple, physically motivated prescription to assign a density threshold above which gas remains self-shielded, which we briefly summarize here (see also Miralda-Escudé et al. 2000; Furlanetto & Oh 2005). Assuming that the typical size of an H I absorber is the Jeans scale and adopting the case A recombination

Table 1. The four background photoionization rates used in this work. The resulting volume-weighted neutral hydrogen fractions (which include the contribution from self-shielded gas) are summarized in the second column.

$\log(\Gamma_{\rm H\,I}/{\rm s}^{-1})$	$\langle f_{\rm H\,I}\rangle_{\rm V}$
−12.8	2.7×10^{-3}
−13.2	9.2×10^{-3}
−13.6	3.2×10^{-2}
−14.0	1.1×10^{-1}

coefficient for ionized hydrogen (Abel et al. 1997), the overdensity at which an H I absorber begins to self-shield may be approximated as

$$\Delta_{\rm ss} = 36\,\Gamma_{-12}^{2/3} T_4^{2/15} \left(\frac{\mu}{0.61}\right)^{1/3} \left(\frac{f_{\rm e}}{1.08}\right)^{-2/3} \left(\frac{1+z}{8}\right)^{-3}, \quad (1)$$

where $\Gamma_{-12} = \Gamma_{\rm H\,I}/10^{-12}\,{\rm s}^{-1}$ is the background photoionization rate, $T_4 = T/10^4$ K is the gas temperature, μ is the mean molecular weight and $f_{\rm e} = n_{\rm e}/n_{\rm H}$ is the free electron fraction with respect to hydrogen. Absorbers at this density threshold have a characteristic size

$$L_{\rm ss} = 8.7\,{\rm pkpc}\,\Gamma_{-12}^{-1/3} T_4^{13/30} \left(\frac{\mu}{0.61}\right)^{-2/3} \left(\frac{f_{\rm e}}{1.08}\right)^{1/3}. \quad (2)$$

The fiducial values adopted for $f_{\rm e}$ and μ correspond to a plasma of ionized hydrogen and singly ionized helium. Note that helium is not expected to be doubly ionized until $z \sim 3$ (e.g. Furlanetto & Oh 2008; McQuinn et al. 2009). Comparison to radiative transfer calculations indicate that this simple prescription recovers the density at which intergalactic gas self-shields to within a factor of 2 at $z = 6$ (McQuinn et al. 2011).

We shall consider four different values for the background photoionization rate in this work: $\log(\Gamma_{\rm H\,I}/{\rm s}^{-1}) = -12.8$, -13.2, -13.6 and -14.0. These are summarized in Table 1 along with the corresponding volume-weighted H I fractions. This range is chosen so that the largest value is comparable to recent photoionization rate measurements from the Lyα forest at $z = 6$ (Calverley et al. 2011; Wyithe & Bolton 2011). The lowest value produces a volume-averaged H I fraction of around 10 per cent (with $\Delta_{\rm ss} \sim 2$), and thus approaches the regime where this self-shielding prescription ceases to provide an adequate description[1] of the spatial distribution of H I in the IGM.

Fig. 1 displays the resulting distribution of neutral hydrogen in a two-dimensional slice of the simulation. The self-shielding threshold given by equation (1) is computed self-consistently using the temperatures and densities from the hydrodynamical simulation. Neutral hydrogen (shaded white) traces the densest parts of the cosmic web, and fills a progressively larger fraction of the simulation volume as the amplitude of the ionizing background is lowered.

[1] In other words, when the IGM is no longer in the 'post-overlap' stage of reionization (cf. Gnedin 2000) and neutral gas also resides in underdense regions far from ionizing sources. This self-shielding model only applies to what is sometimes referred to as the final 'outside-in' stages of reionization (e.g. Miralda-Escudé et al. 2000; Choudhury et al. 2009; Finlator et al. 2009).

2.3 Extracting line-of-sight quantities

We use these neutral hydrogen distributions as the starting point for constructing mock Lyα absorption spectra. Sightlines are extracted parallel to the box boundaries in three directions around the 100 most massive dark matter haloes in the simulation at $z = 7$. These halo sightlines are spliced together with sightlines drawn randomly from the periodic volume to form a total of 300 continuous skewers through the density, peculiar velocity and temperature field of the hydrodynamical simulation. The skewers have a total length of 12.5 pMpc, ranging from 8330 to $-2084\,{\rm km\,s}^{-1}$ around the halo position. The Lyα optical depth along each of the sightlines is then computed following a standard procedure, see e.g. equation (15) in Bolton & Haehnelt (2007a). In the rest of our analysis, all quantities will be estimated from these 300 sightlines.

We note, however, that the most massive dark matter halo in the simulation volume at $z = 7$ has a mass $M_{\rm dm} = 9.0 \times 10^9\,{\rm M}_\odot$. In comparison, Ouchi et al. (2010) infer an average dark matter host halo mass of 10^{10}–10^{11} ${\rm M}_\odot$ from the clustering of LAEs with $L_{{\rm Ly}\alpha} > 2.5 \times 10^{42}\,{\rm erg\,s}^{-1}$ at $z = 6.6$. Our simulation is therefore too small to correctly sample typical LAE host haloes while simultaneously resolving the small-scale structure of the IGM, so in what follows we will underestimate the impact of the more extended gas overdensities and/or stronger inflows expected around larger haloes on the visibility of the Lyα emitters. However, both of these effects will tend to make the impact of Lyα absorption on the visibility of the Lyα emitters stronger, rather than weaker, serving to strengthen our main conclusion that modest H I fractions may explain the observed LAE fraction at $z = 7$.

3 PROPERTIES OF THE OPTICALLY THICK ABSORBERS

It is instructive to first make contact with observations by comparing our simulation results at $z = 7$ to constraints from the IGM at $z \leq 6$. The upper panel in Fig. 2 displays the four photoionization rates used in Fig. 1. The filled symbols in the middle panel display the corresponding volume-averaged H I fractions predicted by these models. The lowest H I fraction is consistent with only weak evolution from the lower observational limit at $z = 6$, whereas smaller photoionization rates result in a stronger increase in the H I fraction towards $z = 7$. Note that these H I fractions are higher than the values expected if self-shielding were ignored – this is demonstrated by the open symbols at $z \sim 7$, which display the H I fraction computed from our simulated sightlines without the self-shielding prescription given by equation (1) (i.e. assuming a uniform, optically thin ionizing background).

The bottom panel of Fig. 2 displays the resulting number density of absorption systems with column[2] densities $10^{17.2} \leq N_{\rm H\,I}/{\rm cm}^{-2} \leq 10^{20.0}$, along with the recent observational measurements presented by Songaila & Cowie (2010) at $z \leq 6$. The filled (open) symbols again display the results including (excluding) self-shielding. Lowering the amplitude of the H I ionizing background significantly increases the incidence of these absorption systems. This increase is more pronounced in the models incorporating self-shielding, with a factor of ∼25 increase in the number density of absorbers per unit redshift from $\log(\Gamma_{\rm H\,I}/{\rm s}^{-1}) = -12.8$ to -14.0.

[2] Column densities are estimated by integrating the density field over a scale of 20 pkpc; this choice is motivated by equation (2), which yields $L_{\rm ss} \simeq$ 16–40 pkpc for the range of photoionization rates considered here.

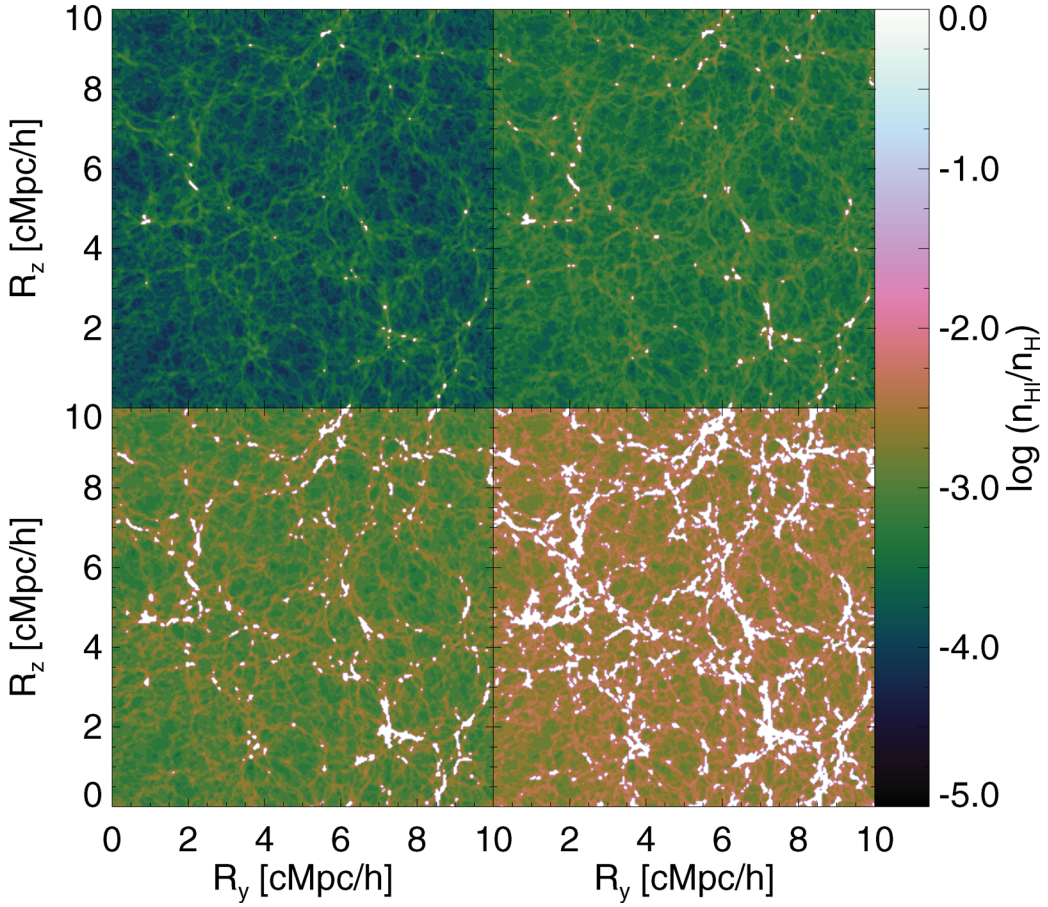

Figure 1. Slices mid-way ($R_x = 5\,h^{-1}$ cMpc, with width $\Delta R_x = 39\,h^{-1}$ ckpc) through the hydrodynamical simulation volume at $z = 7$ displaying the spatial distribution of the neutral hydrogen fraction, $n_{\rm H\,I}/n_{\rm H}$, for four different background photoionization rates. A self-shielding prescription (see equation 1) has been used in all four cases. Fully neutral self-shielded regions, which trace the highest density regions in the simulation, are shaded white. Anticlockwise from top left, $\log(\Gamma_{\rm H\,I}/{\rm s}^{-1}) = -12.8, -13.6, -14.0$ and -13.2.

The absorber properties are displayed in more detail in Fig. 3, where the left-hand panel displays the H I column density distribution functions (CDDFs) obtained from the simulations. The CDDF follows the conventional definition:

$$f(N_{\rm H\,I}, z) = \frac{\partial^2 N}{\partial z \partial N_{\rm H\,I}} \frac{H(z)}{H_0(1+z)^2}. \quad (3)$$

Including self-shielding increases the number of optically thick absorbers, flattening the otherwise power-law column density distribution at $10^{17.2} \leq N_{\rm H\,I}/{\rm cm}^{-2} \leq 10^{19.2}$. A similar flattening of the CDDF is inferred from observations at $z \sim 3.7$ (Prochaska, O'Meara & Worseck 2010), and it has also been noted in many other theoretical models (Katz et al. 1996; Zheng & Miralda-Escudé 2002; Nagamine, Choi & Yajima 2010; Altay et al. 2011; McQuinn et al. 2011). The distributions converge at $N_{\rm H\,I} \sim 10^{20}$ cm^{-2}, indicating that the highest column density systems (damped Lyα absorbers with $N_{\rm H\,I} \geq 10^{20.3}$ cm^{-2}) remain largely insensitive to changes in the background photoionization rate by virtue of their high gas density, at least for $\Gamma_{\rm H\,I} \leq 10^{-12.8}$ s^{-1}. The middle panel in Fig. 3 displays $N_{\rm H\,I} f(N_{\rm H\,I})$, which indicates which optically thick systems comprise the bulk of the H I opacity. When self-shielding is included, it is absorption systems with $N_{\rm H\,I} \sim 10^{18.5}$–$10^{19.5}$ cm^{-2} which dominate.

Finally, the ionization state of the optically thick absorbers is displayed in the right-hand panel of Fig. 3 (see also fig. 5 of McQuinn et al. 2011). The blue diamonds and orange squares show the average H I fraction against column density for $\log(\Gamma_{\rm H\,I}/{\rm s}^{-1}) = -12.8$ and -14.0, respectively. As the photoionization rate is lowered, the density threshold for self-shielding is reduced (since $\Delta_{\rm ss} \propto \Gamma_{-12}^{2/3}$) and the size and incidence rate of optically thick absorption systems (i.e. $N_{\rm H\,I} > \sigma_{\rm H\,I}^{-1} = 10^{17.2}$ cm^{-2}, where $\sigma_{\rm H\,I}$ is the H I photoionization cross-section at the Lyman limit) increase. The self-shielded regions first extend into the outer parts of galactic haloes and then into the filaments defining the cosmic web (e.g. Fig. 1). For comparison, the red triangles display the results obtained for $\log(\Gamma_{\rm H\,I}/{\rm s}^{-1}) = -12.8$ when ignoring self-shielding. Absorbers with the same $N_{\rm H\,I}$ have larger H I fractions when self-shielding is included, implying these must correspond to regions of lower gas density relative to the optically thin case. As we shall now demonstrate, it is this rapid increase in the incidence of optically thick absorption systems with increasing neutral fraction at the tail-end of reionization which is primarily responsible for strengthening the red Lyα damping wing in our simulations.

4 IMPLICATIONS FOR LAE VISIBILITY

4.1 Photoionization by a central source

We now turn to the main result in this paper; estimating the impact of the increasing incidence of optically thick absorbers on the visibility of LAEs. Before proceeding further, however, we also allow for the

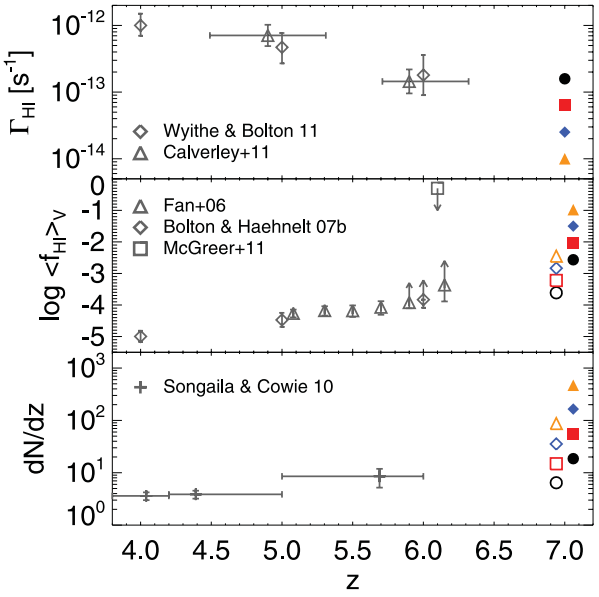

Figure 2. Top: comparison of the four photoionization rates assumed in this work (filled symbols at $z = 7$) with observational constraints at $z \leq 6$ from the Lyα forest opacity (Wyithe & Bolton 2011) and the line-of-sight proximity effect (Calverley et al. 2011). Middle: the filled symbols (offset from $z = 7$ for clarity) display the corresponding volume-averaged H I fraction. The open symbols show the H I fraction which results if self-shielding (see equation 1) is not included. Observational constraints at $z \leq 6.1$ are from IGM Lyα absorption measurements (Fan et al. 2006; Bolton & Haehnelt 2007b; McGreer, Mesinger & Fan 2011). Bottom: the number density of absorption systems with $10^{17.2} \leq N_{\rm H\,I}/{\rm cm}^{-2} \leq 10^{20.0}$ per unit redshift. The filled (open) symbols at $z = 7$ again show the model predictions including (excluding) gas which is self-shielded from the ionizing background. The data points with error bars display the number density of absorbers per unit redshift measured by Songaila & Cowie (2010) at $z < 6$, rescaled to match the cosmological parameters assumed in this work.

possible effect of ionizing radiation from a central source in our models (i.e. the Lyα emitter under observation). Ionizing radiation from the LAE itself can reduce the incidence of proximate self-shielded gas and therefore weaken the Lyα damping wing.

We model the possible effect of the LAE as follows. First, we compute the emission rate of ionizing photons into the IGM, $\dot{N}_{\rm ion}$ (s^{-1}), by an LAE with observed Lyα luminosity $L_{{\rm Ly}\alpha}$ assuming case B recombination:

$$\dot{N}_{\rm ion} = \frac{3}{2}\frac{L_{{\rm Ly}\alpha}}{h_{\rm P}\nu_\alpha}\frac{f_{\rm esc}}{(1-f_{\rm esc})f_\alpha}. \quad (4)$$

Here, the energy of an Lyα photon is $h_{\rm P}\nu_\alpha = 10.2$ eV, and $f_{\rm esc}$ and f_α are the escape fractions of Lyman continuum and Lyα photons into the IGM. In this work we follow Dijkstra, Lidz & Wyithe (2007) and assume $f_\alpha = 1$, such that $L_{{\rm Ly}\alpha} = f_\alpha L^{\rm intr}_{{\rm Ly}\alpha}$ yields the Lyα luminosity uncorrected for dust. We adopt $L_{{\rm Ly}\alpha} = 5 \times 10^{42}$ erg s^{-1} based on the typical Lyα luminosities measured in recent observations of $z \sim 7$ LAEs (e.g. Pentericci et al. 2011). We assume a Lyman continuum escape fraction of $f_{\rm esc} = 0.2$, which yields $\dot{N}_{\rm ion} = 1.1 \times 10^{53}$ s^{-1}. The Lyman continuum escape fraction is highly uncertain. A value $\gtrsim$20 per cent is required at $z \simeq 6$ if the observed LBG population is to reproduce ionizing background constraints from the Lyα forest (Bolton & Haehnelt 2007b; Finkelstein et al. 2012; Shull et al. 2012), but as we will discuss in more detail in Section 4.4 the relation between Lyα emission and the escape of ionizing radiation may not be straightforward.

In the models with a central ionizing source, we then assume the total photoionization rate to be the sum of the LAE contribution and the metagalactic background rate,

$$\Gamma^{\rm tot}_{\rm H\,I}(R) = \sigma_{\rm H\,I}\frac{\dot{N}_{\rm ion}}{4\pi R^2}\frac{\beta}{\beta+3} + \Gamma_{\rm H\,I}, \quad (5)$$

where we have assumed a power-law spectral energy distribution for the ionizing radiation from the LAE, $L_\nu \propto \nu^{-\beta}$, with $\beta = 3$ (cf. Leitherer et al. 1999). Note that we have (i) ignored the finite lifetime of the LAE, effectively assuming that the ionizing radiation propagates instantaneously along the line of sight, (ii) ignored the intervening H I opacity between self-shielded systems and (iii) assumed that the LAE luminosity is constant. All three assumptions will maximize the impact of ionizing radiation from the LAE on the surrounding neutral hydrogen. In what follows, we therefore consider this as a limiting case and bracket other possibilities by additionally computing the Lyα damping wing when the LAE is ignored. We do not explicitly account for the possible clustering

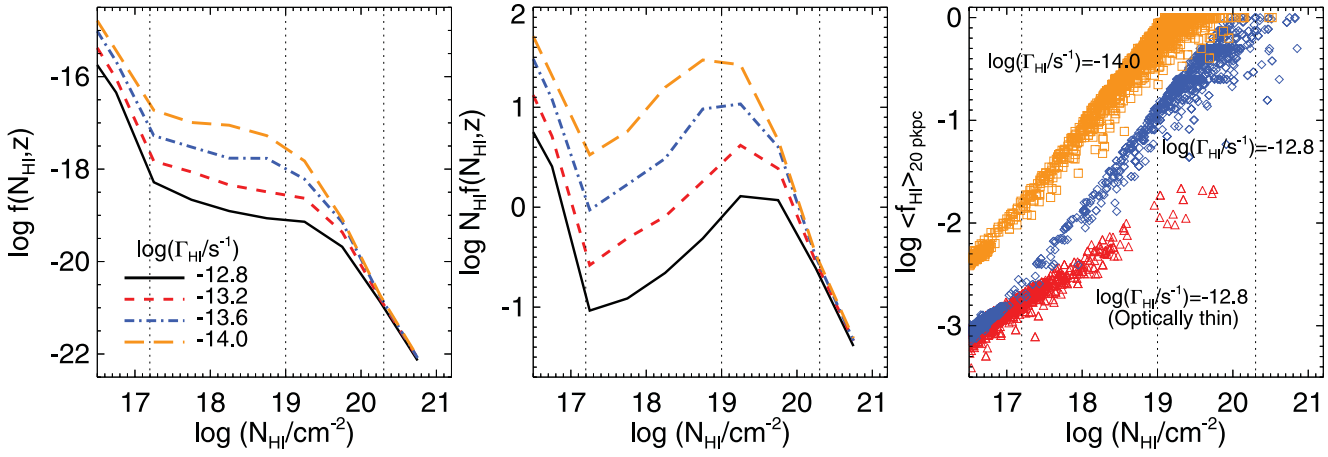

Figure 3. Left: CDDF predicted at $z = 7$ for the four different background ionization rates indicated on the plot. The vertical dotted lines demarcate the column density thresholds by which we define LLSs ($10^{17.2} \leq N_{\rm H\,I}/{\rm cm}^{-2} < 10^{19.0}$), super-LLSs ($10^{19.0} \leq N_{\rm H\,I}/{\rm cm}^{-2} < 10^{20.3}$) and damped Ly$\alpha$ absorbers ($N_{\rm H\,I} \geq 10^{20.3}$ cm^{-2}). Middle: same as for the left-hand panel, but now displaying log $N_{\rm H\,I} f(N_{\rm H\,I})$. Right: scatter plots of absorber H I fractions against H I column density for the largest and smallest of the ionization rates assumed. The red triangles show the results obtained when self-shielding is ignored for $\log(\Gamma_{\rm H\,I}/{\rm s}^{-1}) = -12.8$ only.

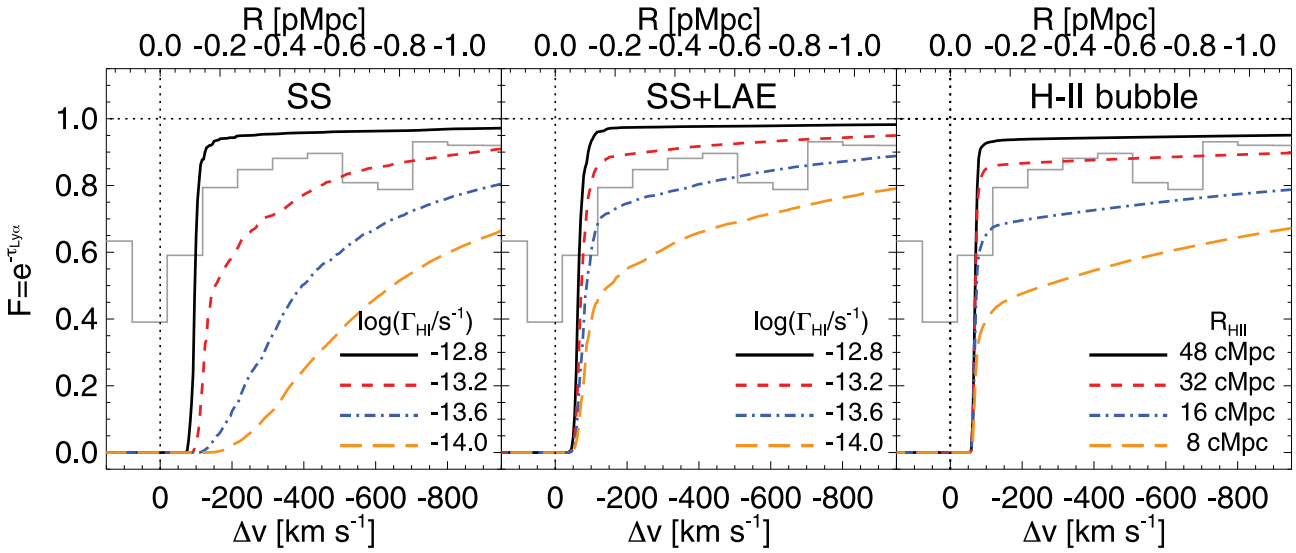

Figure 4. The median Lyα transmission redward of the rest-frame Lyα transition (at $\Delta v = 0\,\mathrm{km\,s^{-1}}$) obtained from an ensemble of 300 simulated sightlines. Each panel displays a different intergalactic Lyα absorption model. The four continuous curves in each panel display the transmission profile for different background ionization rates as indicated. The binned grey line displays the observed transmitted fraction around the $z = 7.085$ quasar ULAS J1120+0641 with an estimated $\dot{N}_{\rm ion} = 1.3 \times 10^{57}\,\mathrm{s^{-1}}$. Left: model which includes self-shielded (SS) gas, but ignores the influence of a central ionizing source. Centre: same as for the left-hand panel, but now each sightline includes the photoionization rate from an LAE with $L_{\rm Ly\alpha} = 5 \times 10^{42}\,\mathrm{erg\,s^{-1}}$ which emits ionizing photons at a rate $\dot{N}_{\rm ion} = 1.1 \times 10^{53}\,\mathrm{s^{-1}}$. Right: a model which neglects optically thick systems, and instead models the ionization state of the IGM as an ionized bubble with radius $R_{\rm H\,II}$ embedded in an otherwise fully neutral IGM. The H II bubble sizes are as indicated on the plot. Note that this case is shown to emulate results from existing models in the literature only.

of ionizing sources around the LAE in addition to the range of background photoionization rates we already consider. As we shall demonstrate in the next section, larger background photoionization rates weaken the red Lyα damping wing by raising the density threshold at which gas self-shields.

4.2 The red Lyα damping wing

Fig. 4 displays the median IGM Lyα transmission profile obtained from the 300 simulated sightlines – each panel corresponds to a different IGM absorption model. Note that when computing the transmission profiles we have ignored the contribution of all gas within 20 pkpc of the centre of the LAE host halo to both the Lyman continuum and Lyα opacity. We do not model the complex radiative transfer within the host galaxy's interstellar medium, and account for the absorption by this material with the parameters $f_{\rm esc}$ and f_α instead.

The left-hand panel shows the transmission profile predicted by our simulations without photoionization by the LAE. A strong damping wing profile is produced, even for photoionization rates that correspond to H I fractions as low as $\sim$3 per cent (blue dot–dashed curve). This is due to the presence of high column density Lyman limit systems (LLS) or damped Lyα absorption systems within $\sim$1 pMpc of the LAE host halo (at $\Delta v = 0\,\mathrm{km\,s^{-1}}$). For comparison, the grey binned line in all panels displays the transmission profile of the $z = 7.085$ quasar ULAS J1120+0641 (Mortlock et al. 2011); a strong damping wing extends redwards of systemic Lyα despite the expected quasar proximity effect and the fact that the biased regions where bright quasars form should reionize earlier than on average. This implies that if similar ionization conditions hold around bright LAEs at $z = 7$, an even stronger red damping wing may result.

The central panel instead shows the damping wings for our models including ionizing emission from an LAE. The source dominates the total photoionization rate (i.e. produces more than 50 per cent of the total) within $\sim$0.5 pMpc. The incidence of proximate, self-shielded systems within this radius is therefore significantly reduced, and the Lyα damping wing is consequently weakened. On the other hand, recall that the typical halo mass in our simulations is rather small (see Section 2.3). We therefore likely underestimate the abundance of proximate optically thick systems and this effect may be somewhat less important. The convergence of the transmission profiles at $F = 0$ (close to $\Delta v = -50\,\mathrm{km\,s^{-1}}$) is due to peculiar velocities arising from gravitational infall around the haloes. We have verified that ignoring peculiar motions produces profiles which converge at $\Delta v = 0\,\mathrm{km\,s^{-1}}$ instead. Note that in the left-hand panel of Fig. 4, where emission from a central LAE is excluded, this convergence is less prominent. This is because absorption line cores from proximate absorbers in addition to the Lyα damping wing can extend redward of systemic Lyα; this occurs more frequently as the photoionization rate is lowered and the size of the absorbers increases.

At this point, it is important to emphasize that the transmission profiles also vary significantly between individual sightlines; a strong damping wing will occur whenever there are super-LLS or damped Lyα absorbers lying close to the host halo. This can occur even when the IGM is highly ionized [i.e. for $\log(\Gamma_{\rm H\,I}/\mathrm{s^{-1}}) = -12.8$] assuming that a sufficiently overdense region lies in close proximity to the LAE. This variation can be seen clearly in Fig. 5, which shows the 68 and 95 per cent bounds for the scatter around the median Lyα absorption profile for $\log(\Gamma_{\rm H\,I}/\mathrm{s^{-1}}) = -12.8$ (upper panel) and -14.0 (lower panel). Some Lyα emitters will therefore be completely obscured by the damping wing while others will remain fully visible. The stochastic nature of the damping wing absorption from these high column density systems should therefore also impact on the clustering of LAEs (e.g. Furlanetto et al. 2006; McQuinn et al. 2007a) for even relatively low H I fractions of 3–10 per cent, modifying the enhanced clustering signal expected as the

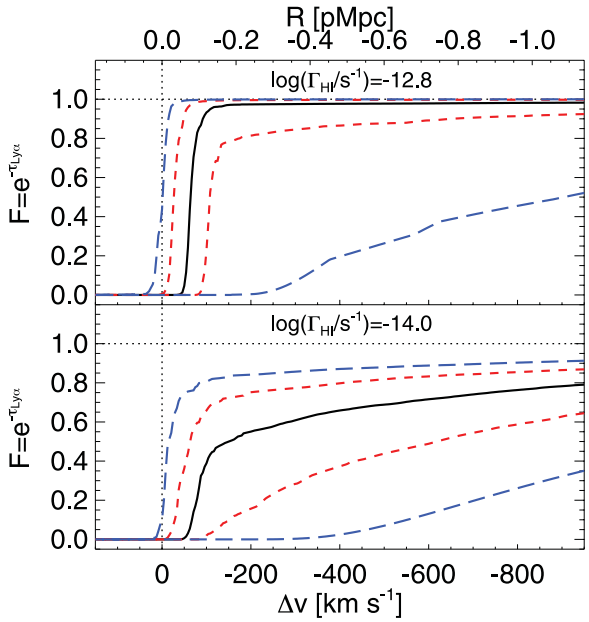

Figure 5. The scatter in Lyα transmission along individual sightlines. Each panel assumes the background photoionization rates indicated on the diagram and includes a central ionizing source with $\dot{N}_{\rm ion} = 1.1 \times 10^{53}\,{\rm s}^{-1}$. The short-dashed (red) and long-dashed (blue) curves bound 68 and 95 per cent of the Lyα transmission around the median (black curves). Note that the median profiles are identical to those displayed in the central panel of Fig. 4.

IGM H I fraction rises. This will be an interesting possibility to explore in future work.

In summary, it is clear that optically thick absorbers can produce a rapid decline in the transmission of Lyα emission from high-redshift galaxies at the tail-end of reionization. This is quite different from existing predictions using large-scale numerical and semi-analytical simulations of reionization. In the late stages of reionization, the presence of self-shielded regions where hydrogen can recombine and stay neutral is very important (Miralda-Escudé et al. 2000; Ciardi et al. 2006; Gnedin & Fan 2006; Choudhury et al. 2009; Crociani et al. 2011; Alvarez & Abel 2012). Large-scale reionization simulations do not yet have the dynamic range to resolve these systems (see e.g. Trac & Gnedin 2011). Any neutral gas is thus typically far away from the central regions of H II regions, and the impact of nearby optically thick absorbers on the Lyα damping wing is ignored.

We illustrate this in the right-hand panel of Fig. 4, where we have simulated the Lyα damping wing expected around an LAE embedded in an H II bubble with radius $R_{\rm H\,II}$. Inside the bubble ($R \leq R_{\rm H\,II}$), the IGM is highly ionized with a uniform H I fraction of 10^{-4}, while outside the IGM is fully neutral. This simple model serves to illustrate the importance of optically thick absorbers for the red damping wing. Bubble sizes of $R_{\rm H\,II} \lesssim 30$ cMpc are required to produce a damping wing similar in strength to the absorption seen when the IGM is only ∼3 per cent neutral by volume (blue dot–dashed curve in the central panel of Fig. 4) when including optically thick absorbers. In comparison, large-scale reionization simulations typically predict H II bubble sizes of ∼30–40 cMpc for H I fractions as large as 30 per cent (e.g. fig. 2 in Zahn et al. 2011). This elucidates why existing models indicate that the LAE/LBG fraction at $z \sim 7$ may imply large H I fractions of 40–90 per cent. At fixed neutral fraction, large-scale reionization simulations predict a damping wing which is significantly weaker compared to the case where absorption by optically thick absorbers is included. The damping wing will therefore only reduce LAE visibility at times when individual H II bubbles have not yet grown to the typical size of $\gtrsim$50 cMpc reached at overlap in these simulations.

4.3 The REW distribution

We now compare our models directly to recent measurements of the LBG/LAE fraction (Fontana et al. 2010; Pentericci et al. 2011; Vanzella et al. 2011; Ono et al. 2012; Schenker et al. 2012) following the approach of Dijkstra et al. (2011), which we recapitulate here. Our first requirement is to compute the fraction of the Lyα emission line which is transmitted, $\mathscr{T}$, where

$$\mathscr{T} = \frac{\int_{\nu_{\rm min}}^{\nu_{\rm max}} {\rm d}\nu\, J(\nu) {\rm e}^{-\tau_{{\rm Ly}\alpha}(\nu)}}{\int_{\nu_{\rm min}}^{\nu_{\rm max}} {\rm d}\nu\, J(\nu)}. \quad (6)$$

Here, $J(\nu)$ gives the shape of the Lyα line profile, ${\rm e}^{-\tau_{{\rm Ly}\alpha}(\nu)}$ is the IGM transmission (e.g. Fig. 4), and $\nu_{\rm min}$ and $\nu_{\rm max}$ are chosen to correspond to the full extent of our simulated sightlines. To compute $\mathscr{T}$ for each of our simulated sightlines, we must assume an intrinsic Lyα profile. We adopt a Gaussian line profile with a standard deviation of 88 km s^{-1}, corresponding to the circular velocity of a dark matter halo of mass $10^{10}\,{\rm M}_\odot$ at $z = 7$ (equation 25 in Barkana & Loeb 2001). We further assume that the line centre is shifted redward of Lyα by 400 km s^{-1}; this offset is typical of Lyα emission lines associated with LBGs at $z \simeq 2$–3 (Steidel et al. 2010), and is chosen to mimic the effect of resonant scattering by the (outflowing) gas on the Lyα line visibility (but see our discussion in the next section).

We next construct a probability distribution ${\rm d}P(<\log \mathscr{T})/{\rm d}\log \mathscr{T}$ for each IGM absorption model using our simulations. For Lyα redshifted relative to systemic we assume the observed rest-frame equivalent width (REW) at $z = 6$, when the hydrogen in Universe is already highly ionized, to be equal to the emitted REW (i.e. $\mathscr{T}_{z=6} = 1$). If we further assume that there is no intrinsic evolution in the LAE population from $z = 6$ to 7, the cumulative probability distribution (CPDF) that a galaxy has an observed REW and an IGM transmission $\mathscr{T}$ at $z = 7$ is

$$P(>{\rm REW}) = \int_0^1 {\rm d}\mathscr{T} \frac{{\rm d}P(<\log \mathscr{T})}{{\rm d}\log \mathscr{T}} \frac{P_{z=6}(>{\rm REW}/\mathscr{T})}{\mathscr{T} \ln 10}. \quad (7)$$

Here, ${\rm REW_{intr}} = {\rm REW}/\mathscr{T}$, $P_{z=6}(>{\rm REW}) = \exp(-{\rm REW}/{\rm REW_c})$ and ${\rm REW_c} = 50$ Å (see Dijkstra et al. 2011 for details).

Fig. 6 displays the resulting CPDFs for the IGM models with self-shielding only (left-hand panel) and including ionization by a central LAE (central panel). Note again that these two cases have been chosen to bracket the uncertain impact of Lyman continuum emission from the central LAE on the surrounding IGM (see also the discussion in Section 4.4). The CPDFs are compared to a recent data compilation presented by Ono et al. (2012), as well as an upper limit at 75 Å from Stark et al. (2010). All curves in the central panel lie above the quoted observational uncertainties, implying that a lower line-of-sight escape fraction ($f_{\rm esc} < 0.2$) is required to match the data if the H I fraction remains fixed. As expected, however, our simulations do predict a rapid evolution in the REW distribution from $z = 6$, even for modest neutral fractions of 3 per cent (blue dot–dashed curve). In the right-hand panel, the CPDF for the $\log(\Gamma_{\rm H\,I}/{\rm s}^{-1}) = -14.0$ model in the central panel (orange long-dashed curve with $\langle f_{\rm H\,I}\rangle_{\rm V} \sim 0.1$) is shown assuming four different offsets for the Lyα emission line relative to systemic. Shifting the line blueward (redward) of the fiducial −400 km s^{-1} decreases

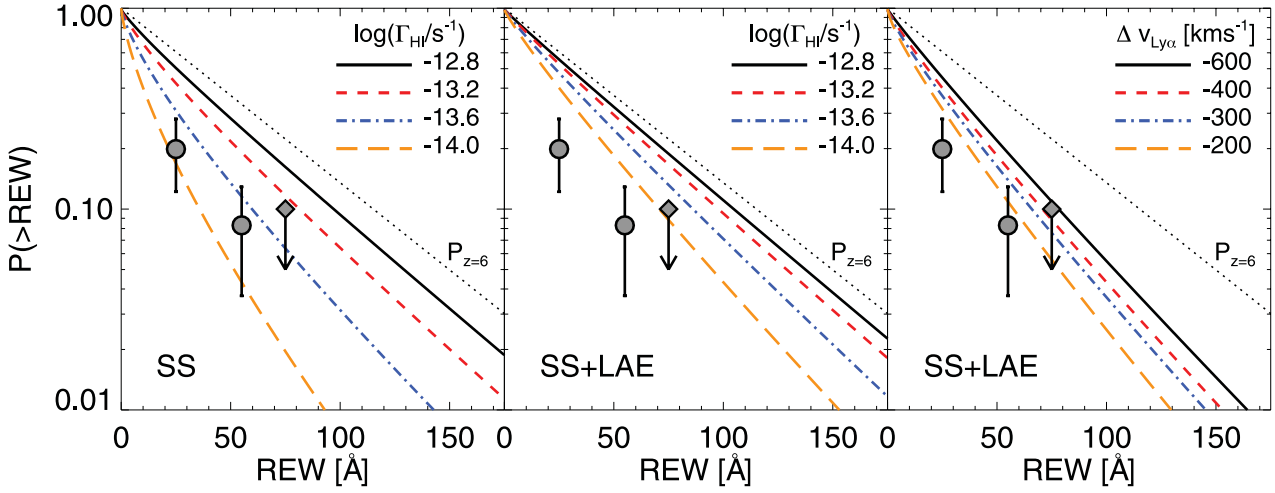

Figure 6. Predicted cumulative probability distributions (CPDFs) for the rest-frame Lyα equivalent width (REW) at $z = 7$. The dotted curves display the intrinsic $z = 6$ CPDF assuming that the IGM is fully transparent to Lyα photons (Dijkstra et al. 2011). The solid, short-dashed, dot–dashed and long-dashed curves are constructed from our Lyα transmission models at $z = 7$ excluding (left) and including (centre) ionizing radiation emitted along the line of sight from a source with $L_{\rm Ly\alpha} = 5 \times 10^{42}\,{\rm erg\,s^{-1}}$ and $\dot{N}_{\rm ion} = 1.1 \times 10^{53}\,{\rm s^{-1}}$ (see the text for details). These models adopt an intrinsic REW distribution identical to that at $z = 6$ and differ due to evolution in the Lyα transmission only. A Gaussian Lyα profile with a standard deviation of 88 km s^{-1} and an offset of $-400\,{\rm km\,s^{-1}}$ redward of rest-frame Lyα has been assumed in both cases. The right-hand panel instead displays the $\log(\Gamma_{\rm H\,I}/{\rm s^{-1}}) = -14.0$ case from the central panel (with $\langle f_{\rm H\,I}\rangle_{\rm V} \sim 0.1$) assuming four different Lyα emission line offsets. The models are compared to the composite data set compiled by Ono et al. (2012) (filled circles) which utilizes observations from Fontana et al. (2010), Vanzella et al. (2011), Pentericci et al. (2011) and Schenker et al. (2012). The upper limit at 75 Å is based on the earlier non-detection by Stark et al. (2010) at $z \sim 7$.

(increases) $\mathscr{T}$, producing a stronger (weaker) evolution in the REW distribution.

4.4 Uncertainties

From our discussion thus far, it should be clear that modelling the IGM transmission for LAEs at the tail-end of reionization is uncertain mainly because of the difficulties with self-consistently modelling self-shielded regions. However, uncertainties associated with the escape of ionizing radiation from the (possibly clustered) Lyα emitters and the redshift relative to systemic of the Lyα emission also play a role.

When including an LAE in our models we have assumed $f_{\rm esc} = 0.2$. It is, however, not obvious that high-redshift galaxies emit ionizing and Lyα radiation at the same time and/or in the same direction. It is certainly plausible that no ionizing radiation escapes in the direction of the observer (e.g. Gnedin, Kravtsov & Chen 2008), in which case even our IGM model excluding a central source (i.e. the left-hand panel in Fig. 6) may actually be an overestimate of the IGM transmission $\mathscr{T}$; recall that we have ignored all neutral gas within 20 pkpc of the halo centre and instead assumed the appropriate escape fractions for ionizing and Lyα photons. Note further that the escape of ionizing radiation and the emission redshift relative to systemic may also be unfavourably coupled. A large redshift for the emission line may need a large column density of neutral gas within the host halo of the LAE. This is required in order to resonantly scatter the Lyα photons locally far into the red wing of the line (e.g. Barnes et al. 2011). The redshifts of 400 km s^{-1} or more for the observed Lyα emission in $z = 3$ LBGs (Steidel et al. 2010) may therefore be incompatible with a simultaneous escape of ionizing radiation along the line of sight to the observer.

The detailed intrinsic line Lyα shape is also rather uncertain – in this work we have assumed a simple Gaussian line profile with standard deviation 88 km s^{-1}. In practice, however, radiative transfer models predict a characteristic double-peaked emission line (e.g. Verhamme, Schaerer & Maselli 2006) with intergalactic Lyα absorption removing the blue peak at high redshift. In their recent analysis of the REW distribution predicted by large-scale reionization simulations, Jensen et al. (2012) adopt a doubled-peaked Gaussian minus a Gaussian line based on the radiative transfer simulations presented by Laursen et al. (2011). They note that using this line profile weakens the impact of the H I fraction on the REW distribution compared to a simple Gaussian centred at the systemic redshift. Note, however, since we adopt a profile which is shifted redward of systemic, our assumption that the entire line is visible in the absence of a red Lyα damping wing is reasonable. Unless the line width becomes comparable to the line offset relative to systemic, this will not have a significant effect on the resulting REW distribution.

Lastly, the small simulation box size of $10\,h^{-1}$ cMpc and the omission of self-consistent modelling for the ionizing sources remains the most significant concern in this analysis. We do not correctly model large-scale variations in the IGM ionization state prior to overlap. On the other hand, we argue that the proper modelling of dense, self-shielded regions is an equally important part of this problem. A fully self-consistent model will require combining both of these aspects, either by resolving all relevant physical scales or adopting subgrid models which are informed by high-resolution simulations of the IGM density field. Furthermore, any modelling should be calibrated to reproduce the observed transmission redwards of Lyα in bright high-redshift quasars which appears to evolve rapidly between $z = 6$ and 7; the simulations presented here have been used to estimate a neutral fraction of >10 per cent around the $z = 7.085$ quasar ULAS J1120+0641 (e.g. Bolton et al. 2011; Mortlock et al. 2011). Note, however, that this is based on a small number of bright quasars at $z \sim 6$ and only one at $z > 7$. Future observations will help determine whether ULAS J1120+0641 is typical.

5 CONCLUSIONS

We have used a hydrodynamical simulation to model the Lyα opacity of the intervening IGM during the final stages of reionization. As the photoionization rate drops, the opacity redward of rest-frame Lyα is expected to rise rapidly due to the increasing incidence of optically thick absorption systems. Our results indicate that the bulk of the H I opacity will arise from optically thick systems with column densities $N_{\rm H\,I} \sim 10^{18.5}$–$10^{19.5}\,{\rm cm}^{-2}$. When including these absorption systems in the simulations, only a moderate rise in the volume-averaged neutral fraction is required to significantly reduce the transmission redward of rest-frame Lyα.

This result has an important implication for the interpretation of the recently observed decline in the Lyα emission from high-redshift galaxies at $z \sim 6$–7 (e.g. Stark et al. 2010; Hayes et al. 2011; Pentericci et al. 2011; Curtis-Lake et al. 2012; Ono et al. 2012; Schenker et al. 2012). We find that these observations do not require a large neutral fraction (∼40–90 per cent) in the intervening IGM at $z = 7$ as previously suggested. Instead, if the rapid decline in the LAE/LBG fraction is further corroborated, it may instead be indicative of the rapid decrease of the mean free path of ionizing photons expected at the tail-end of reionization. Furthermore, as we find the Lyα emission from high-redshift galaxies will be suppressed for volume-averaged neutral fractions of only 3–10 per cent, the patchiness of reionization may produce a more modest impact on the clustering properties of observable high-redshift LAEs than previously predicted.

Our findings may be particularly relevant for future surveys which plan to use the transmission of Lyα emission and the clustering properties of LAEs to probe deep into the epoch of reionization. Detecting these LAEs at $z > 7$ may well become difficult, even when the IGM is only 10 per cent neutral. It may also mean that spectroscopic confirmation of high-redshift candidate galaxies identified with the dropout technique at $z > 7$ may become problematic, at least until emission lines other than Lyα can be observed with the *James Webb Space Telescope*. Finally, extending theoretical predictions beyond the approximate approach adopted in this work is vital. This will ultimately require incorporating small-scale absorption systems into simulations which also model the patchy nature of reionization on large scales. This remains a considerable but fundamental computational challenge for the current generation of reionization simulations.

ACKNOWLEDGMENTS

The hydrodynamical simulation used in this work was performed using the Darwin Supercomputer of the University of Cambridge High Performance Computing Service (http://www.hpc.cam.ac.uk/), provided by Dell Inc. using Strategic Research Infrastructure Funding from the Higher Education Funding Council for England. We thank Volker Springel for making GADGET-3 available, and Mark Dijkstra, Zoltan Haiman and Matt McQuinn for helpful comments on the draft manuscript. Fig. 1 utilizes the cube helix colour scheme introduced by Green (2011). JSB acknowledges the support of an ARC post-doctoral fellowship (DP0984947), and thanks Pratika Dayal and Stuart Wyithe for valuable conversations.

REFERENCES

Abel T., Anninos P., Zhang Y., Norman M. L., 1997, New Astron., 2, 181
Altay G., Theuns T., Schaye J., Crighton N. H. M., Dalla Vecchia C., 2011, ApJ, 737, L37
Alvarez M. A., Abel T., 2012, ApJ, 747, 126
Barkana R., Loeb A., 2001, Phys. Rep., 349, 125
Barnes L. A., Haehnelt M. G., Tescari E., Viel M., 2011, MNRAS, 416, 1723
Becker G. D., Rauch M., Sargent W. L. W., 2007, ApJ, 662, 72
Bolton J. S., Haehnelt M. G., 2007a, MNRAS, 374, 493
Bolton J. S., Haehnelt M. G., 2007b, MNRAS, 382, 325
Bolton J. S., Haehnelt M. G., Warren S. J., Hewett P. C., Mortlock D. J., Venemans B. P., McMahon R. G., Simpson C., 2011, MNRAS, 416, L70
Calverley A. P., Becker G. D., Haehnelt M. G., Bolton J. S., 2011, MNRAS, 412, 2543
Choudhury T. R., Haehnelt M. G., Regan J., 2009, MNRAS, 394, 960
Ciardi B., Scannapieco E., Stoehr F., Ferrara A., Iliev I. T., Shapiro P. R., 2006, MNRAS, 366, 689
Ciardi B., Bolton J. S., Maselli A., Graziani L., 2012, MNRAS, 423, 558
Crociani D., Mesinger A., Moscardini L., Furlanetto S., 2011, MNRAS, 411, 289
Curtis-Lake E. et al., 2012, MNRAS, 422, 1425
Dayal P., Maselli A., Ferrara A., 2011, MNRAS, 410, 830
Dijkstra M., Wyithe J. S. B., 2010, MNRAS, 408, 352
Dijkstra M., Lidz A., Wyithe J. S. B., 2007, MNRAS, 377, 1175
Dijkstra M., Mesinger A., Wyithe J. S. B., 2011, MNRAS, 414, 2139
Fan X. et al., 2006, AJ, 132, 117
Finkelstein S. L. et al., 2012, ApJ, 758, 93
Finlator K., Özel F., Davé R., Oppenheimer B. D., 2009, MNRAS, 400, 1049
Fontana A. et al., 2010, ApJ, 725, L205
Forero-Romero J. E., Yepes G., Gottlöber S., Prada F., 2012, MNRAS, 419, 952
Furlanetto S. R., Oh S. P., 2005, MNRAS, 363, 1031
Furlanetto S. R., Oh S. P., 2008, ApJ, 681, 1
Furlanetto S. R., Zaldarriaga M., Hernquist L., 2004, ApJ, 613, 1
Furlanetto S. R., Zaldarriaga M., Hernquist L., 2006, MNRAS, 365, 1012
Gnedin N. Y., 2000, ApJ, 535, 530
Gnedin N. Y., Fan X., 2006, ApJ, 648, 1
Gnedin N. Y., Kravtsov A. V., Chen H.-W., 2008, ApJ, 672, 765
Green D. A., 2011, Bull. Astron. Soc. India, 39, 289
Haardt F., Madau P., 2001, in Neumann D. M., Tran J. T. V., eds, Clusters of Galaxies and the High Redshift Universe Observed in X-rays, preprint (arXiv:astro-ph/0106018)
Haiman Z., 2002, ApJ, 576, L1
Haiman Z., Spaans M., 1999, ApJ, 518, 138
Hansen M., Oh S. P., 2006, MNRAS, 367, 979
Hayes M., Schaerer D., Östlin G., Mas-Hesse J. M., Atek H., Kunth D., 2011, ApJ, 730, 8
Hu E. M., Cowie L. L., Barger A. J., Capak P., Kakazu Y., Trouille L., 2010, ApJ, 725, 394
Iliev I. T., Mellema G., Pen U.-L., Merz H., Shapiro P. R., Alvarez M. A., 2006, MNRAS, 369, 1625
Jeeson-Daniel A., Ciardi B., Maio U., Pierleoni M., Dijkstra M., Maselli A., 2012, MNRAS, 424, 2193
Jensen H., Laursen P., Mellema G., Iliev I. T., Sommer-Larsen J., Shapiro P. R., 2012, MNRAS, in press (arXiv:1206.4028)
Kashikawa N. et al., 2006, ApJ, 648, 7
Katz N., Weinberg D. H., Hernquist L., Miralda-Escude J., 1996, ApJ, 457, L57
Kohler K., Gnedin N. Y., 2007, ApJ, 655, 685
Komatsu E. et al., 2011, ApJS, 192, 18
Kuhlen M., Faucher-Giguère C.-A., 2012, MNRAS, 423, 862
Laursen P., Sommer-Larsen J., Razoumov A. O., 2011, ApJ, 728, 52
Lawrence A., 2007, MNRAS, 379, 1599
Leitherer C. et al., 1999, ApJS, 123, 3
McGreer I. D., Mesinger A., Fan X., 2011, MNRAS, 415, 3237
McQuinn M., Hernquist L., Zaldarriaga M., Dutta S., 2007a, MNRAS, 381, 75
McQuinn M., Lidz A., Zahn O., Dutta S., Hernquist L., Zaldarriaga M., 2007b, MNRAS, 377, 1043

McQuinn M., Lidz A., Zaldarriaga M., Hernquist L., Hopkins P. F., Dutta S., Faucher-Giguère C.-A., 2009, ApJ, 694, 842
McQuinn M., Oh S. P., Faucher-Giguère C.-A., 2011, ApJ, 743, 82
Malhotra S., Rhoads J. E., 2004, ApJ, 617, L5
Mesinger A., 2010, MNRAS, 407, 1328
Miralda-Escudé J., 1998, ApJ, 501, 15
Miralda-Escudé J., Rees M. J., 1998, ApJ, 497, 21
Miralda-Escudé J., Haehnelt M., Rees M. J., 2000, ApJ, 530, 1
Mortlock D. J. et al., 2011, Nat, 474, 616
Nagamine K., Choi J.-H., Yajima H., 2010, ApJ, 725, L219
Ono Y. et al., 2012, ApJ, 744, 83
Ouchi M. et al., 2010, ApJ, 723, 869
Pawlik A. H., Schaye J., van Scherpenzeel E., 2009, MNRAS, 394, 1812
Pentericci L. et al., 2011, ApJ, 743, 132
Prochaska J. X., O'Meara J. M., Worseck G., 2010, ApJ, 718, 392
Santos M. R., 2004, MNRAS, 349, 1137
Schaye J., 2001, ApJ, 559, 507
Schenker M. A., Stark D. P., Ellis R. S., Robertson B. E., Dunlop J. S., McLure R. J., Kneib J.-P., Richard J., 2012, ApJ, 744, 179
Shull J. M., Harness A., Trenti M., Smith B. D., 2012, ApJ, 747, 100
Songaila A., Cowie L. L., 2010, ApJ, 721, 1448
Springel V., 2005, MNRAS, 364, 1105
Stark D. P., Ellis R. S., Chiu K., Ouchi M., Bunker A., 2010, MNRAS, 408, 1628
Steidel C. C., Erb D. K., Shapley A. E., Pettini M., Reddy N., Bogosavljević M., Rudie G. C., Rakic O., 2010, ApJ, 717, 289
Trac H., Cen R., 2007, ApJ, 671, 1
Trac H. Y., Gnedin N. Y., 2011, Adv. Sci. Lett., 4, 228
Vanzella E. et al., 2011, ApJ, 730, L35
Verhamme A., Schaerer D., Maselli A., 2006, A&A, 460, 397
Wyithe J. S. B., Bolton J. S., 2011, MNRAS, 412, 1926
Wyithe J. S. B., Bolton J. S., Haehnelt M. G., 2008, MNRAS, 383, 691
Zahn O., Lidz A., McQuinn M., Dutta S., Hernquist L., Zaldarriaga M., Furlanetto S. R., 2007, ApJ, 654, 12
Zahn O., Mesinger A., McQuinn M., Trac H., Cen R., Hernquist L. E., 2011, MNRAS, 414, 727
Zheng Z., Miralda-Escudé J., 2002, ApJ, 568, L71
Zheng Z., Cen R., Trac H., Miralda-Escudé J., 2011, ApJ, 726, 38

This paper has been typeset from a TEX/LATEX file prepared by the author.